Nanoscale

Accepted Manuscript

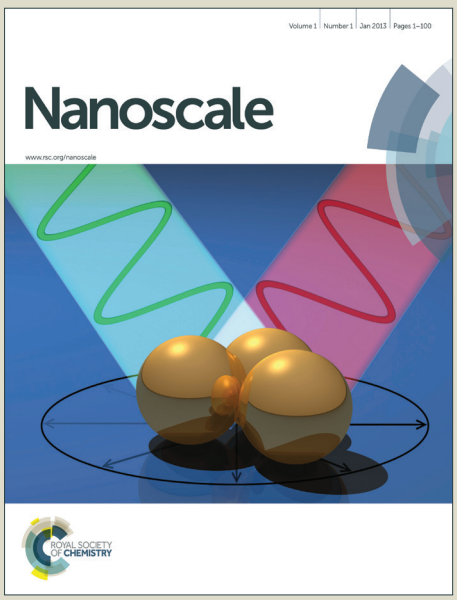

ROYAL SOCIETY OF CHEMISTRY

www.rsc.org/nanoscale

Iron oxide superparamagnetic nanoparticles conjugated with a conformationally blocked α-Tn antigen mimetic for macrophage activation.

Massimo Manuelli,[§] Silvia Fallarini,[∇]Grazia Lombardi,[∇] Claudio Sangregorio, [#, §, ϒ] Cristina Nativi,[§,]* and Barbara Richichi[§]

§ Dipartimento di Chimica "U. Schiff" and INSTM, Università di Firenze, via della Lastruccia 3, Sesto Fiorentino, I-50019 Firenze, Italy, # Istituto di Scienze e Tecnologie Molecolari, Consiglio Nazionale delle Ricerche, via C. Golgi 19, I-20133 Milano, Italy, and ∇ Dipartimento di Scienze del Farmaco, Università del Piemonte Orientale "Amedeo Avogadro", L.go Donegani 2, I-28100 Novara, Italy

* Address correspondence to
cristina.nativi@unifi.it

ϒ Present address: Istituto di Chimica dei Composti Organo-Metallici, Consiglio Nazionale delle Ricerche, via Madonna del Piano, 10, Sesto Fiorentino, I-50019 Firenze, Italy.

ABSTRACT. Among new therapies to fight tumors, immunotherapy still is one of the most promising and intriguing. Thanks to the ongoing structural elucidation of several tumor antigens and the development of innovative antigen carriers, immunotherapy is in constant evolution and it is largely used either alone or in synergy with chemotherapy/radiotherapy. With the aim to develop fully synthetic immunostimulants we have recently developed a mimetic of the α-Tn mucin antigen, a relevant tumor antigen. The $^4C_1$ blocked mimetic **1**, unique example of α-Tn

mimetic antigen, was functionalized with an ω-phosphonate linker and used to decorate iron oxide superparamagnetic nanoparticles (MNPs), employed as multivalent carriers. MNPs, largely exploited for supporting and carrying biomolecules, like antibodies, drugs or antigens, consent to combine in the same nanometric system the main features of an inorganic magnetic core with a bioactive organic coating. The superparamagnetic glyconanoparticles obtained, named **GMNPs**, are indeed: biocompatible, immunoactive, and preserve the proper characteristics for their use as heat mediators in the magnetic fluid hyperthermia (MFH) treatment of tumors. All together these properties make **GMNPs** attracting devices for innovative tumor treatment.

KEYWORDS: immunotherapy · α-Tn antigen · magnetic nanoparticles · magnetic fluid hyperthermia · macrophage activation

In the last decade, thanks to the accumulation of knowledge on the molecular mechanisms involved in immune modulation, immunotherapy has emerged as a powerful strategy in the enduring fight against tumors. In the meanwhile, the development of antigen-specific therapeutic vaccines by using fully-characterized synthetic antigens, as immunogens, became the very ultimate goal in this domain. Tumors uniquely or excessively express antigens (tumor-associated antigens; TAAs) and, in particular, glycan antigens (tumor-associated carbohydrate antigens; TACAs), which can be useful targets for vaccines. TACAs are indeed widely exposed on cancer cell surfaces and their expression often correlates with cancer developmental stages, including invasion and metastasis. Furthermore, an abnormal glycosylation in the primary tumors is considered a signal of poor prognosis.[1]

Despite the large numbers of TAAs/TACAs so far described, their use in tumor therapy

remains limited and needs improvements. This not only because immune responses in cancer patients can be relatively weak, but also because TACAs are poorly immunogenic antigens. Moreover, most TACAs are recognized as *self* and, according to their saccharidic nature, they cannot be presented to T cells for T cell responses (T cell-independent type II antigens). Consequently, the class switch from IgM to IgG and the recall memory response, are not generated.[2]

A successful strategy to overcome these limiting aspects might be mimicking the natural multivalent approach of the molecular biosystems by binding carbohydrate antigens to multivalent scaffolds, such as nanomaterials. TACA multivalent display, indeed, mimicking the natural multivalent carbohydrates presentation on cell surface, can lead to B cell activation and antibody production.[3] Furthermore, a nanomaterial, as antigen delivery system, can provide an adjuvant activity, inducing activation and maturation of antigen presenting cells (APCs)[4] and promoting antigen cross-presentation.[5] Overall, these are essential events for inducing an efficient antitumor immune response.

A variety of natural and synthetic scaffolds, including proteins,[6,7] dendrimers,[8] silica and gold nanoparticles,[9] has been recently proposed for the multivalent presentation of specific epitopes to the immune cells. Among them, the use of superparamagnetic iron oxide nanoparticles (MNPs) are particularly appealing, as they offer several advantages. Suitably coated MNPs are, indeed, biocompatible and present a rich chemical reactivity of their surface, that can be exploited for binding to antibodies, drugs or saccharides (functionalized MNPs). Functionalized MNPs, do combine in the same nanometric system the required features to be used in early tumor diagnosis and treatment, as well as in tumor monitoring and tracking by magnetic resonance imaging.[10] As a matter of fact, the heat they can release by the application of an

external magnetic alternating field at a proper radio-frequency (50-500 kHz) can be exploited in the treatment of tumors (magnetic fluid hyperthermia, MFH).

Recently, MFH has gained a great attention from researchers in the field for clinical trials currently underway, clearly showed the efficacy of this therapy when combined with radiotherapy at low-dosage in the treatment of glioblastoma, pancreas and prostate tumors.[11,12] In the last five years the number of works reporting on novel MNP-based heat mediators coated with stealth polymers, drugs or targeting moieties rapidly increased, and very recent reports highlighted that MFH, beside inducing tumor cell death due to the increasing of temperature in the surrounding tissues, can contribute to the activation of the immune system against cancer.[13]

The synergistic combination of the stimulation of tumor-bearing host immune responses with a localized heating may, therefore, pave the way towards the realization of novel and more efficient multimodal anticancer agents.

In this work, we present the synthesis and characterization of a novel multivalent glycoconjugate nanosystem, composed of ferrimagnetic biocompatible iron oxide MNPs functionalized with the epitope **1**, a structurally blocked mimetic of the α-Tn antigen expressed in carcinoma-associated mucins. Mucins are heavily *O*-glycosylated extracellular proteins forming a major part of protective biofilm on epithelial cells and providing a protective barrier against dangerous compounds. Mucin over expression often matches the pathogenesis of cancer, particularly of adenocarcinomas, and harmfully influences cellular growth, differentiation, transformation, adhesion, and also the immune surveillance.[14]

Mucins, when abnormally over expressed, can undergo an under gycosylation giving rise to tumor-associated epitopes, such as α-Tn (αGalNAc), TF (Galβ(1,3)-α-GalNAc) and their sialylated forms, which are expressed on the surface of tumor cells and which can be exploited

for immunotherapy. As a matter of fact, though TACAs are generally weakly immunogenic, α-Tn, sialylated α-Tn (sTn), and TF antigens, displayed strong immunogenicity and, as some of the other specific tumor antigens, they have been used for developing carbohydrate-based anticancer vaccines.[15] In particular, the α-Tn antigen due to its structural simplicity has been a privileged synthetic target for vaccine development.[16]

In normal cells, the α–Tn structure is hidden for further glycosylation. Conversely, in most human carcinomas it is exposed at the surface as consequence of the incomplete formation of the saccharidic chain. Like in normal cells, however, tumor cell-associated mucins are characterized by a high level of glycosylation and an high expression of the Tn antigen α-*O*-linked to a serine (Ser) and/or threonine (Thr) residue, as first aminoacid of the polypeptide backbone. α-*O*-Glycosylation has a dramatic organizational effect on the antigenic peptide backbone, forcing it into an extended conformation.[17] Thus, the main challenge of any synthetic approach reported for the α-Tn antigen, as well as for their peptidic derivatives, was represented by the stereoselective formation of the α-glycosidic linkage between GalNAc and Ser/Thr derivatives.[18]

Relying on the efficient inverse electron-demand Diels-Alder reaction between glycals and the α,α'-dioxothiones[19] obtained from aspartic acid, some years ago we reported on the diasteroselective synthesis of the Tn-like compound **1** which maintains the key structural features of such natural α-*O*-glycopeptide and presents suitable functional groups for the elongation of the aminoacidic chain or the insertion of a desired linker and/or carrier.[20] The structurally rigid compound **1**, preserves the $^4C_1$ conformation and is recognized by *Viscumin Album Agglutinin* (VAA), a lectin which selectively binds galactose residues, and competes with

lactose, a common ligand for VAA known to enter the lectin sites, in competitive STD experiments.[20] (Figure 1)

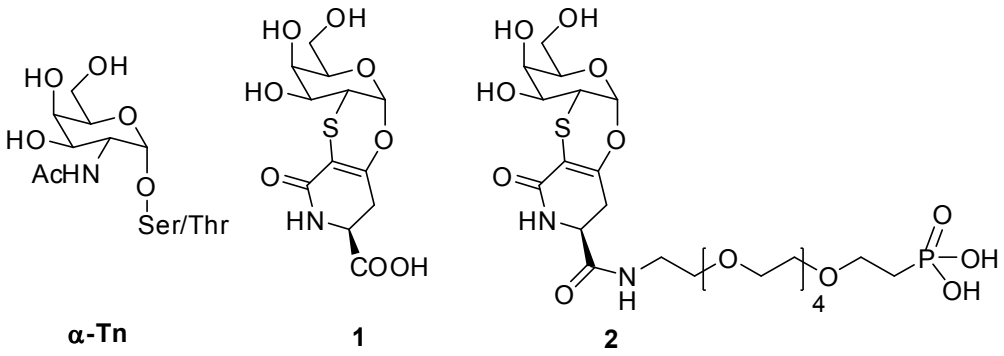

Figure 1. Structure of α-Tn antigen and α-Tn-like derivatives **1** and **2**.

With the aim of preparing a novel multivalent glycoconjugate nanosystem decorated with the α-Tn-like residues **1**, the compound **2** was synthesized. This latter presents an hexaethylene glycol linker with a terminal phosphonate function suitable for the anchorage of the α-Tn-like epitopes **1** to magnetite/maghemite MNPs with an average diameter of 11 nm.

The investigation of the structural, magnetic and hyperthermic properties of the glycosyl MNPs obtained, **GMNPs**, confirmed the successful decoration of the MNP surface with the epitope **2**, and revealed that the inorganic cores owned the proper magnetic characteristics to be used for clinical applications as heat mediators in the MFH treatment of tumors.

The **GMNPs** were then biologically evaluated for purity, biocompatibility, cellular uptake, and immunoactivity. In particular, *in vitro* tests were performed for glucosyl MNPs (**GlcMNPs,** *i.e.* MNPs decorated with glucose residues, as negative control), the **GMNPs**, the monovalent epitope **2**, the citrate-coated MNPs, **CMNPs** and the polyethylene glycol-coated MNPs

(**PEMNPs**), also taken as negative control. For each compound we measured: 1) the absence of endotoxin contamination; 2) the effects induced on cell viability after 24-72 h incubation; 3) the cellular uptake; 4) the ability to stimulate immune cell responses. Our results, clearly demonstrating that the **GMNPs** under evaluation are biocompatible and immunoactive, may contribute to a better understanding of the biological properties and applicability of MNPs.

RESULT AND DISCUSSION

Synthesis of phosphonate derivative 2. The compound **2** was prepared using the galactoside **3** as starting material.[20] which was firstly treated with freshly prepared tetrabutylamonium hydrogen fluoride (TBAHF) to remove the silylidene protective group, then reacted with acetic anhydride and pyridine to form the peracetylated Tn-like derivative **4**. Removal of the benzyl ester under standard conditions (H_2, Pd/C) afforded the unprotected carboxyl derivative **5**, which, in turn, was reacted with the polyoxygenated amino alcohol **6**[21] in the presence of *O*-(benzotriazol-1-yl)-*N,N,N′,N′*-tetramethyluronium tetrafluoroborate (TBTU) and N-methylmorpholine (NMM) to form **7** in 73% yield. By reaction with carbon tetrabromide and triphenylphosphine, the terminal hydroxyl group of **7** was substituted with a bromine (**8,** 88%); then, by heating **8** in the presence of tris-trimethylsilyl phosphite the corresponding triacetylphoshonate **9** was obtained in quantitative yield. Deprotection of the acetyl groups with a solution of ammonia in methanol afforded the α-*O*-glycosyl phosphonate **2** quantitatively (Scheme 1)

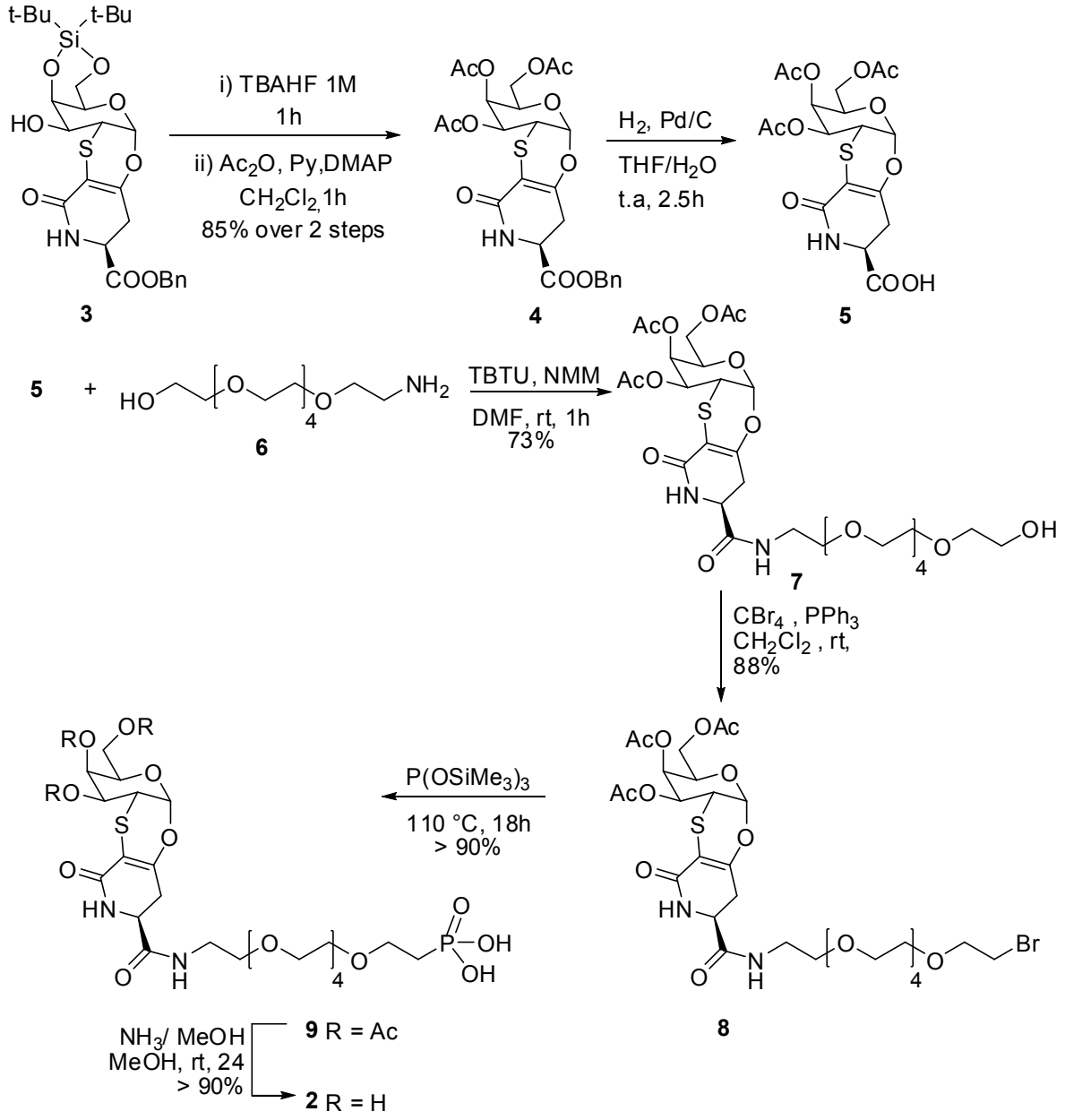

Scheme 1. Synthesis of α-*O*-glycosyl phosphonate **2**.

Synthesis and Decoration of Magnetic Nanoparticles. Magnetite/maghemite MNPs with an average diameter of 11 nm were prepared using a seed-mediated growth process.[22]

First, nearly cubic iron oxide MNPs with an average size of 7.6 ± 0.7 nm, as evaluated from

TEM images (Supporting Information, Figure S1), were obtained by surfactant-assisted thermal decomposition of iron (III) acetylacetonate, $Fe(acac)_3$, in 1-octadecene using oleic acid and oleylamine as surfactants. In the second step, the size of the inorganic core was increased by reacting the former MNPs with more precursor materials under the same experimental conditions. TEM images of the final black product, (Figure 2) shows that the MNPs retain an almost cubic morphology, while the average size calculated along the diagonal increases to

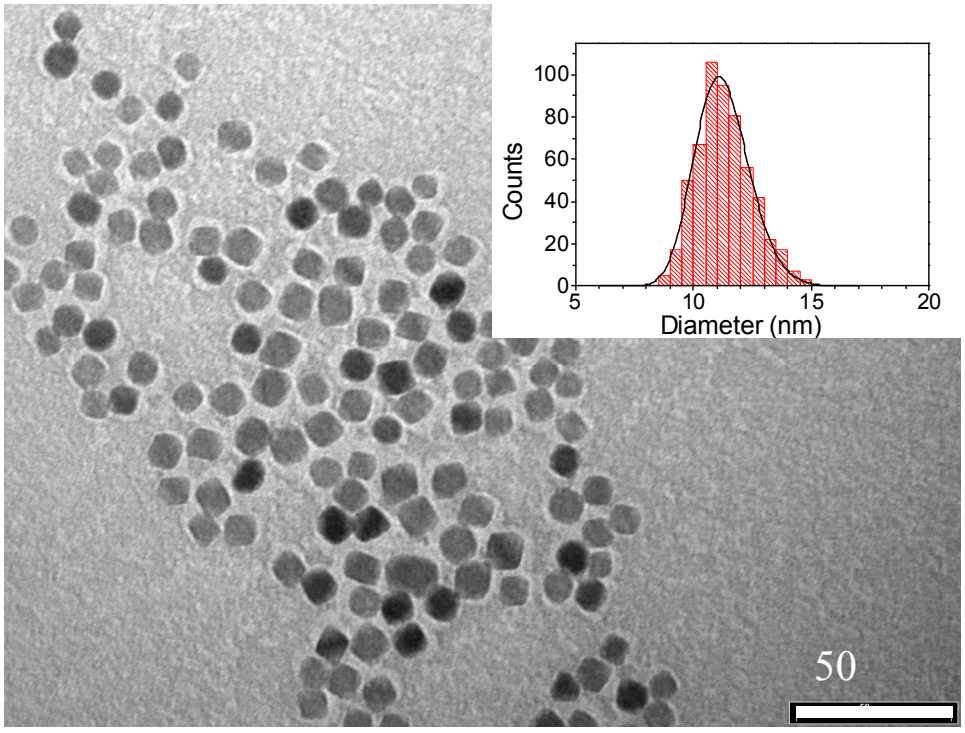

11.3±1.2 nm.

Figure 2. Representative low-magnification TEM image of colloidal magnetite MNPs. The white bar corresponds to 50 nm. In the inset the corresponding size histogram obtained by statistical analysis over ca. 600 MNPs is shown. The continuous black line represents the best fit to a Gaussian.

The position and the relative intensity of all peaks observed in the powder X-Ray Diffraction pattern (Supporting Information, Figure S2) well match those of the *fcc* spinel structure of standard magnetite (JPCDS 19-0629), maghemite (JCPDS 39-1346) or any partially oxidized intermediate ferrite phase, which cannot be easily discriminated from each other. However, the lattice parameter, *a*, is 8.382(5) Å, much closer to that of magnetite (8.396 Å) than to maghemite (8.346 Å). Notably, no evidence of the presence of wüstite, which is often found in iron oxide MNPs prepared by thermal decomposition of iron carboxylates, due to the reducing conditions produced by the precursor decomposition,[23-25] was found in the XRD pattern. The average diameter, evaluated by using the Scherrer's formula, was 11.5±0.8 in a good agreement with the particle sizes observed in TEM images, pointing out the single crystal nature and the high cristallinity of the MNPs.

The magnetic properties of a colloidal solution of the MNPs in heptane were investigated both as a function of temperature and magnetic field. The temperature dependence of the magnetization recorded after zero-field cooling (ZFC) and field-cooling (FC) procedures is reported in Figure 3A. It displays the thermal irreversibility characteristic of an ensemble of randomly oriented single domain MNPs:[26] at room temperature all the particles are in the superparamagnetic regime, consistently with the relatively small size of the MNPs, while below ca. 100 K the two magnetization curves split, indicating the beginning of the freezing process of the MNPs

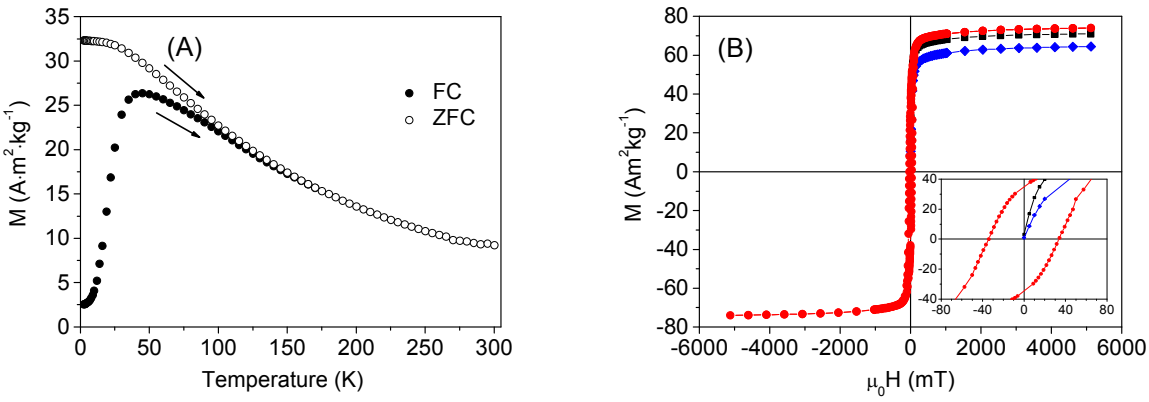

Figure 3. (A) Temperature dependence of the ZFC and FC magnetizations collected on a colloidal solution of the surfactant coated MNPs in heptane with a probe field of 5 mT. (B) Hysteresis loops recorded at 2.5 K (red), 150 K (black) and 300 K (blue curve) and corresponding enlargement of the low field region (inset).

magnetic moment. The blocking temperature, which at first approximation can be identified with the temperature of the maximum of the ZFC curve, was 50 K, which well agrees with that expected for magnetite MNPs of 11-12 nm.[27] Accordingly, an open hysteresis loop with a coercive field, H_C, of 340 Oe, and reduced remnant magnetization, M_{0T}/M_{5T}, equal to 0.49 was measured at low temperature (2.5 K), while no magnetic irreversibility appears when the loops were measured above the blocking temperature (at 150 K and at room temperature, Figure 3B). The magnetization was almost saturated at the highest measuring field of 5 T (the difference between the values measured at 5 T and those extrapolated from the high field data point are ca. 1 %) reaching 75 Am^2/kg at 2.5 K and then slightly decreasing on increasing temperature. The saturation magnetization resulted close to the literature value of the corresponding bulk materials[28] confirming the single crystal nature and the high cristallinity of the inorganic cores. AC susceptibility measurements at variable frequency (1-1000 Hz, Fig. S3) revealed that at

room temperature, at least in the investigated time window, the reversal of the magnetization is mainly driven by the Néel mechanism, rather than by the mechanical rotation of the whole MNPs.

In order to verify the possibility to exploit the final nanosystem also as a heating seed for possible associated hyperthermia-based antitumor therapy we evaluated the heat dissipation efficiency by recording the temperature kinetic curve of the heptane colloidal solution when exposed to an alternating magnetic field with amplitude H_0 = 11.0 kA/m and frequency ν = 183 kHz. The field parameters were set to stay below the human tolerance threshold, commonly assumed to be given by $H_0 \cdot \nu < 2 - 5 \cdot 10^9$ $A \cdot m^{-1} \cdot s^{-1}$.[29] Larger amplitude or frequency may induce deleterious responses of living tissues and undesired side effects.[12] The application of this alternating field on a 1.9 % w/w solution of the MNPs for 5 minutes produced a

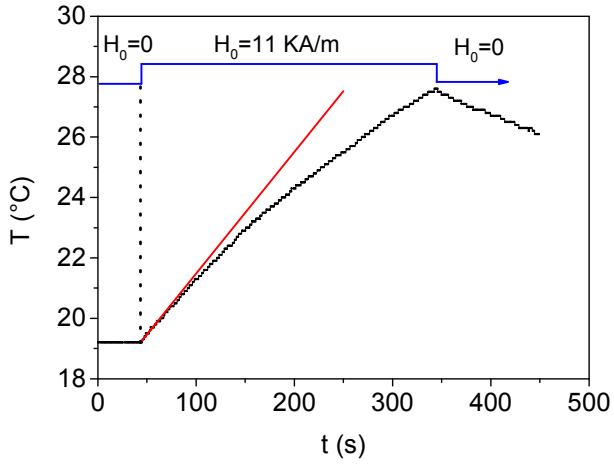

Figure 4. Temperature kinetics of a colloidal solution of iron oxide MNPs during the exposure to the alternating magnetic field (11.0 kA/m, 183 kHz).

sizable temperature increase of ca. 9° C corresponding to a SLP value of ca. 10 W/g, as shown

in Figure 4. Although this value is low if compared to data reported in the literature (which are however, commonly obtained using much higher, clinically unexploitable field amplitudes) it corresponds to a sizable heating efficiency, which suggests this material can be possibly used as heat mediator in adjuvant antitumoral therapy. Moreover, considering the literature data [30] a sharp increase of the hyperthermal efficiency upon a small increase of few nanometers of the MNP average diameter can be envisaged.

The functionalization of the MNPs with the α-Tn-like compound **2** was accomplished by exploiting the large affinity of the phosphonate group for the iron oxide surface.[31,32]

The replacement of the surfactants with the mimetic **2** was accomplished by simple ligand exchange in a chloroform/methanol 10:1 mixture, followed by a second exchange process in water. The final product resulted as a stable black colloidal water solution, as confirmed by DLS measurements (Supporting Information, Figure S4). TEM images showed the inorganic core was unaffected by the functionalization process (Supporting Information, Figure S5A). FTIR spectrum of the ligand exchanged product (Supporting Information, Figure S6), confirmed the substitution of the oleic acid capping agent with the α-Tn mimetic **2**: the two sharp bands at 2922 and 2852 cm^{-1}, observed in the surfactant coated MNPs and attributed to the asymmetric and symmetric CH_2 stretch of the aliphatic chains, respectively, disappeared while at lower wave number (1120 – 950 cm^{-1}) the modes characteristic of the phosphonate group appeared in the spectrum. Of note, the weak band at 990 cm^{-1} which can be attributed to the ν(P-OFe) mode[33] confirmed the grafting of the mimetic on to the ferrite surface occurred through the phosphonate moiety. The characteristic broad envelop at ca. 580 cm^{-1} related to Fe-O bond vibrations was present in both FTIR spectra, indicating the preservation of the iron oxide core after the ligand exchange. The amount of functionalization was estimated from the phosphorous

percentage determined via ICP analysis, and found equal to $2.01 \cdot 10^{-4}$ mmol/mg of MNPs. Assuming an ensemble of identical MNPs with average size and morphology, as indicated by TEM images and density estimated from the XRD pattern, we can evaluate that on average each nanoparticle is grafted by 338 α-Tn-like residues, corresponding to a density of 0.84 molecule/nm^2, which is compatible with an almost complete coating of the iron oxide surface. In order to have a negative control for biological tests, a portion of NP5 was coated, by ligand exchange with citrate molecules (a representative TEM image is shown in Supporting Information, Figure S3b). The replacement of oleic acid with the citrate ligand made the resulting nanoparticles soluble in water.

Biological Tests. Before biologically testing, each compound was carefully evaluated for purity to rule out the possibility that immune cell responses were due to the presence of endotoxin contaminations, such as lypopolysaccharide (LPS), introduced into the system through chemicals, materials or equipments. Limulus amebocyte lysate (LAL) endochrome assays were, thus, performed in four different batches of each compound and the concentration of LPS measured. LPS concentrations were always below the value of 0.01 ng/ml, which is sufficient to stimulate immune cell responses,[34] suggesting that all compounds under testing were LPS-free and biologically evaluable (data not shown).

We, then, studied the effects of **MNPs** on immune cells. For this purpose we decided to use macrophages, since they are potent immune cells providing immediate responses against dangerous molecules and acting as APCs to stimulate adaptive immune responses. Exposure to not self antigens, indeed, can induce a rapid activation of macrophages, which stop proliferation and acquire effector cell functions.[35] For the present study a mouse monocyte/macrophage quiescent cell line (RAW 264.7) was used, since these cells are a widely recognized model of

human macrophages[36] with a good experimental reproducibility. To better evaluate the effect of GMNPs on immune cells, two negative control samples were prepared by coating iron oxide MNPs of the same size with glucosyl (**GlcMNPs**) or polyethylene glycol (9-12 PE units, **PEMNPs**) moieties, respectively. The synthesis and properties of the two samples are described in the Supporting Information.

We analyzed the effects of **GMNPs** and **GlcMNPs** on RAW 264.7 cell viability in comparison to un-functionalized MNPs (**CMNPs** and **PEMNPs**) (controls) and the monovalent α-Tn mimetic **2**. We used three validated *in vitro* assays (Trypan blue, calcein-AM, MTT, see Material and Methods) for toxicity measurements, because it has been demonstrated that MNPs can interfere with several of the well-established methods, originating false-negative results.[37] Cells were exposed to different concentrations (0.01-30 μg/ml) of each compound for 24-72 h; thereafter cell viability was measured. No toxicity was determined in any of the three considered assays at all concentrations tested (Figure 5 and Figure S7, Supporting Information), suggesting that all compounds under evaluation are biocompatible.

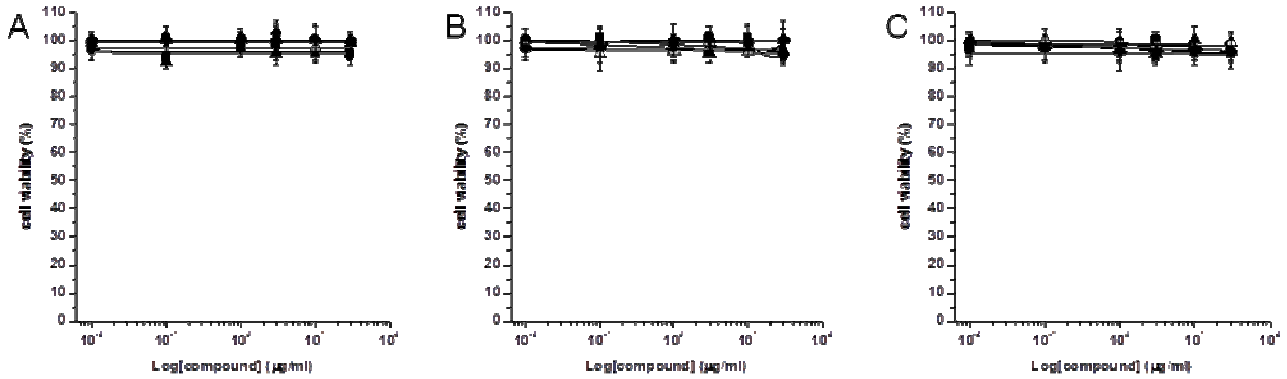

Figure 5. Effects of compound **2**, polyethylene glycol-coated MNPs (**PEMNPs**), citrate-coated MNPs (**CMNPs**), and glycosyl MNPs (**GMNPs** and **GlcMNPs**) on cell viability. RAW 264.7 cells were treated with increasing concentrations (0.01-30 μg/ml) of **2** (closed squares),

PEMNPs (open triangles), **CMNPs** (closed circles), **GMNPs** (closed triangles) or **GlcMNPs** (closed diamonds) for 24h (A), 48h (B) and 72h (C). Cell viability was assessed by MTT. The concentration-response curves show the percentage of cell viability in comparison to controls (compound-untreated cells). The data represent mean ± SEM of at least three independent experiments run in triplicate.

The next step was to qualitatively (Prussian blue staining) investigate the cellular uptake of **CMNPs**, **PEMNPs**, **GlcMNPs** and **GMNPs**. The typical Prussian blue staining images of cells treated with **CMNPs** (A), **GMNPs** (B) or **GlcMNPs** (C) showed an intracellular localization of these MNPs, demonstrating that these MNPs, either glycosylated (B and C) or not (A), can enter into macrophages (Figure 6**).** PEMNPs were not endocyted, while the endocytosis of the α-Tn antigen mimetic **2**, not conjugated to MNPs, cannot be visualized by this method.

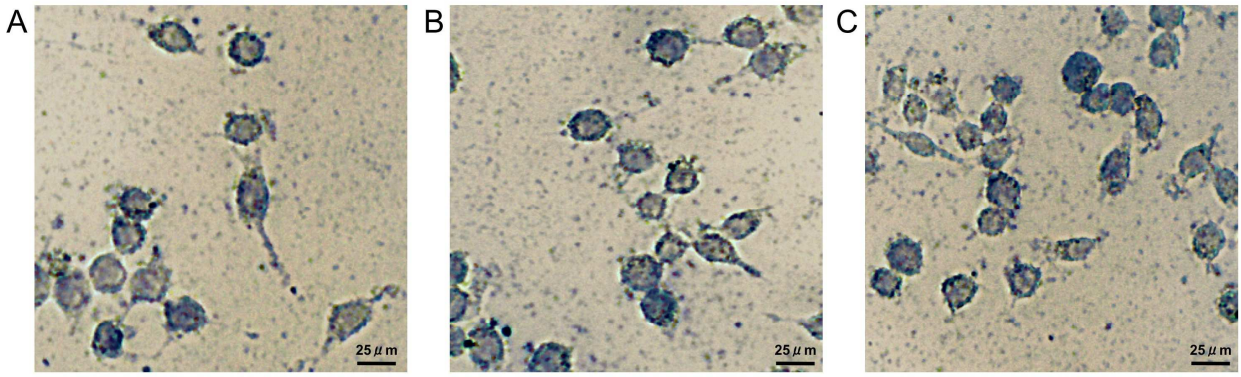

Figure 6. Intracellular MNPs localization. Bright-field images of RAW 264.7 cells treated with 30 μg/ml of **CMNPs** (A), **GMNPs** (B)**,** or **GlcMNPs** (C) for 24h. MNPs were labeled with Prussian blue iron staining and visualized with an optical microscope (objective 40X) equipped with an integrated camera. Images are from a representative experiment carried out three times with similar results (scale bar = 25 μm).

The endocytoses of **2**, **CMNPs**, **PEMNPs**, **GMNPs** and **GlcNMPs** were then quantitatively determined by flow cytometry (FACS). We used side-scattered light (SSC) as an indicator of particle uptake: when particles are endocyted by cells, SSC intensity consequently increases because the cell granularity is enhanced. Figure 7 shows that the SSC intensity increased after cell treatment with MNPs, either functionalized or not, suggesting a similar level of cellular uptake occurs independently on the type of carbohydrate attached to the MNP surfaces. On the contrary, when the cells were exposed to **PEMNPs** or α-Tn mimetic antigen **2**, not conjugated to MNPs, the SSC intensity did not change, demonstrating that they were not endocyted by macrophages (Figure 7).

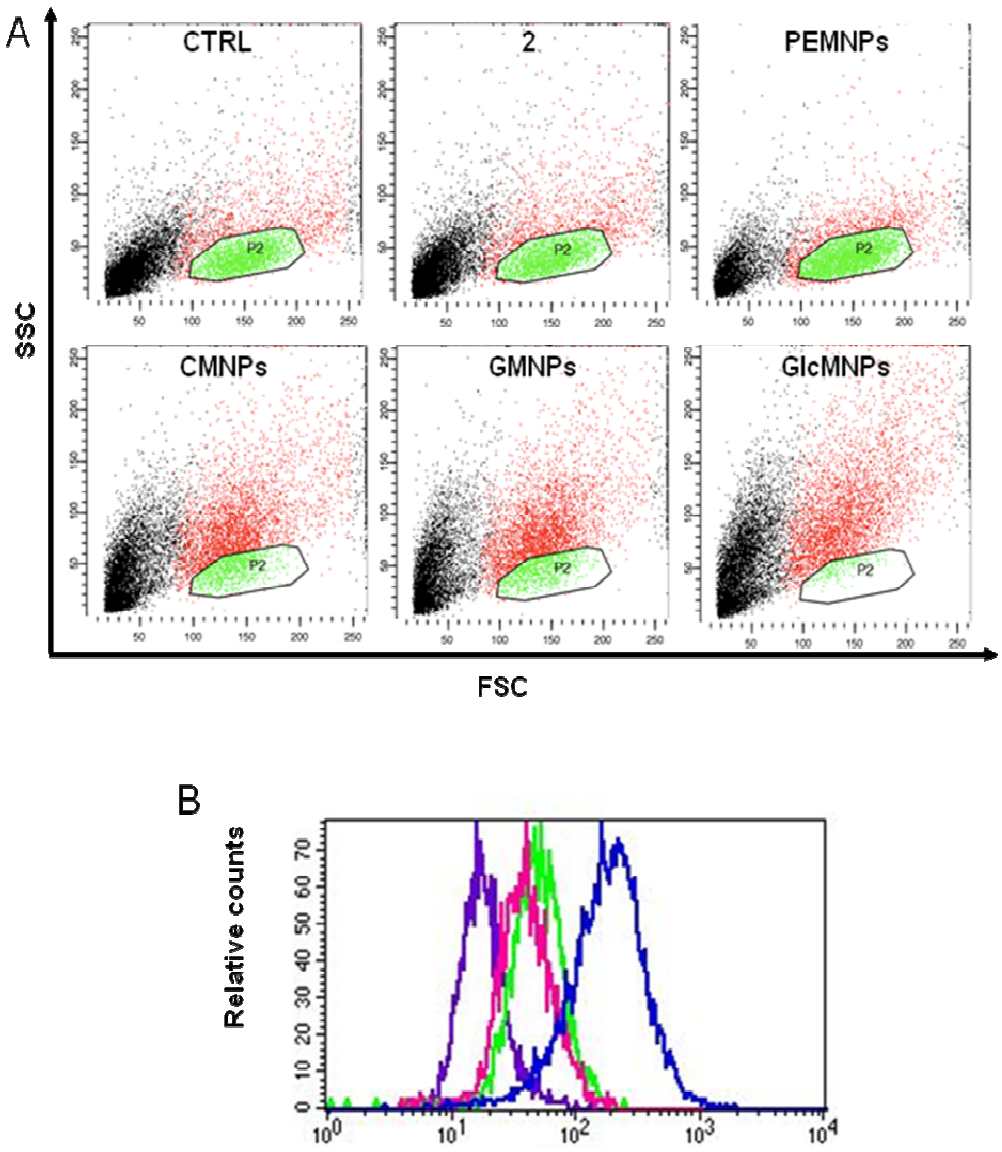

Figure 7. Quantitative evaluation of the **2**, **PEMNPs, CMNPs, GMNPs,** and **GlcMNPs** uptake. RAW 264.7 cells were treated with 30 µg/ml of **2**, **CMNPs, PEMNPs, GMNPs,** or **GlcMNPs** for 24h. The compound uptake was determined by measuring the cell granularity by FACS. (A) Representative dot plots showing the effects of compound uptake on granularity (SSC) and size (FSC) of RAW 264.7 cells. Images are from a representative experiment carried out three times with similar results. (B) Overlay plot of the RAW 264.7 cell SSC measured after **CMNPs** (green), **GMNPs** (pink), or **GlcMNPs** (blue) uptake. Untreated cells are shade in violet.

In agreement with data reported in the literature,[38,39] the peculiar surface properties of the MNPs can explain our results and, in particular, the impact of their charge surface properties on effective phagocytosis. In this sense, the citrate-coated MNPs (**CMNPs**) being negatively charged resulted well internalized by macrophages, while the un-charged polyethylene glycol-coated MNPs (**PEMNPs**) were prevented from cellular uptake. Of note, a multivalent display of the α-Tn mimetic antigen seems to be necessary for macrophage uptake.

Figure 8 and Figure S8 (see Supplementary Information) show the effects of both the concentration and the time of cell exposure to each compound on the levels of MNPs uptake, demonstrating that the type of coating sensibly influences the kinetic of cellular MNPs uptake.

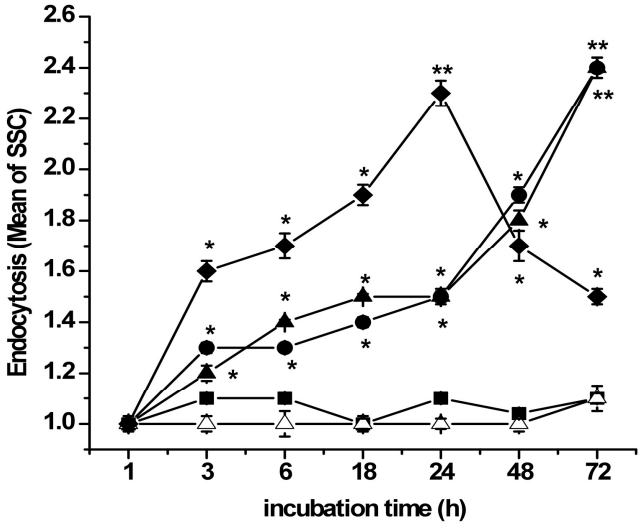

Figure 8. Time-course of **2**, **PEMNPs**, **CMNPs**, **GMNPs** and **GlcMNPs** uptake. RAW 264.7 cells were treated with 30 μg/ml of **2** (closed squares), **PEMNPs** (open triangles), **CMNPs** (closed circles), **GMNPs** (closed triangles) or **GlcMNPs** (closed diamonds) for up to 72 h. At indicated incubation time points, cells were harvested and analyzed. The compound uptake was quantified by FACS. The data represent mean ± SEM of at least three independent experiments. *$p \leq 0.05$; **$p \leq 0.01$ vs. controls (compound-untreated cells).

Finally, we investigated whether MNPs trigger effector functions in the same cells. Figures 9 and 10 show the effects induced by each compound on the production of a typical pro-inflammatory mediator (TNF-α). Remarkably, only the MNPs functionalized with the α-Tn mimetic antigen (**GMNPs**) are able to induce TNF- α gene expression and protein release at levels similar to those obtained with LPS (0.1 μg/ml), while only a 50% of the TNF-α increase was induced by **GlcMNPs** in comparison to **GMNPs**.

The type of the monosaccharide used in the coating influenced not only the levels, but also the time-course of cytokine production: **GMNPs** determined, indeed, a significant time-dependent increase of TNF-α release, while **GlcMNPs** raised a same level of TNF-α releasing, independently of the time considered.

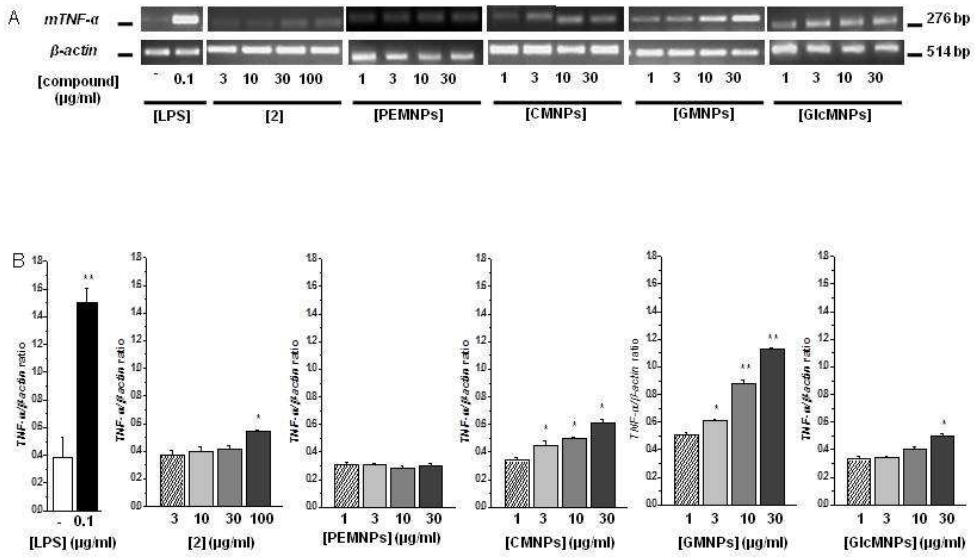

Figure 9. Effects of **2**, **PEMNPs**, **CMNPs**, **GMNPs** and **GlcMNPs** on TNF-α gene expression. RAW 264.7 cells were treated (24h) with increasing concentrations (1-30 μg/ml) of **2**, **PEMNPs**, **CMNPs**, **GMNPs** or **GlcMNPs**, (see Material and Methods and Table 1S, Supplementary Information). Expression of β-actin was used as a loading control. Compound untreated cells (CTRL) were considered as negative, while 0.1 μg/ml LPS-treated cells as positive controls. (A) Representative results of RT-PCR for the TNF-α and β-actin gene expression. (B) The signals were densitometrically analyzed and data, calculated as mean ± SEM of at least three independent determinations, are expressed as ratio (TNF-α/β-actin) of the signals obtained for each sample divided by that obtained for β-actin in the same sample to permit between-sample comparisons. *p≤ 0.05; **p≤0.01 vs. controls (compound-untreated cells).

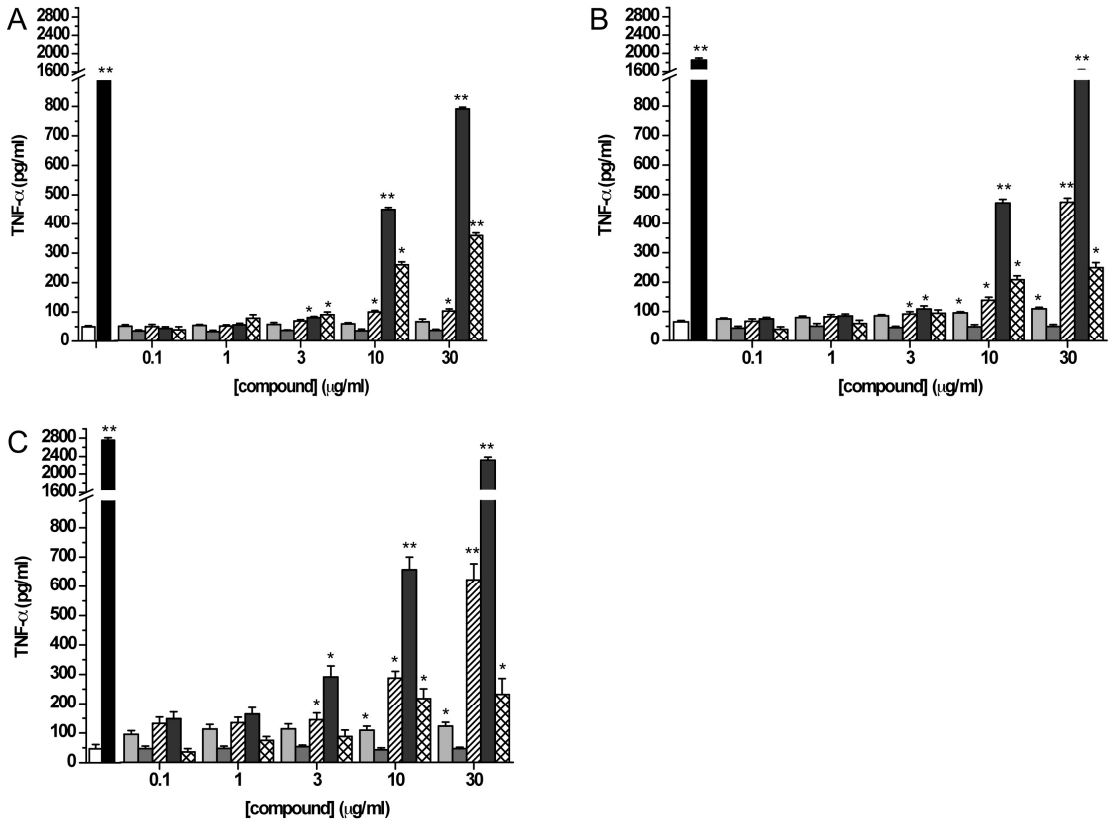

Figure 10. Effects of **2**, **PEMNPs**, **CMNPs**, **GMNPs** and **GlcMNPs** treatment on TNF-α release. RAW 264.7 cells were treated with increasing concentrations (0.1-30 μg/ml) of **2** (light grey bars), **PEMNPs** (grey bars), **CMNPs** (hatched bars), **GMNPs** (dark grey bars) or **GlcMNPs** (cross-hatched bars) for 24h (A), 48h (B) and 72h (C). Compound untreated cells (white bars) were considered as negative, while 0.1 μg/ml LPS-treated cells (black bars) as

positive controls. Supernatants were collected and assayed for TNF-α levels by standard ELISA. The data represent mean ± SEM of at least three independent experiments. *p≤ 0.05; **p≤0.01 vs. controls (compound-untreated cells).

In agreement with data already published by other Authors,[40] our results showed the biological role played in cellular uptake by the monosaccharide used for the MNPs coating. As a matter of fact, it is known[40] that **GlcNPs** are mainly internalized by caveolae-mediated endocytosis, while the galactosyl nanoparticles (**GalNPs**) remain confined on the cell periphery and present a slower internalization kinetic. Although the mechanism of **GMNPs** uptake remains to be clarified, taking into account the structural similarity of the α-Tn mimetic antigen (decorating **GMNPs**) and galactose (decorating **GalNPs**), it is reasonable to suppose that **GMNPs** may follow a cell entrance pattern and processing similar to **GalNP**s.

Overall, these data demonstrate that a multivalent display of α-Tn mimetic antigen is necessary for macrophage activation. Macrophages, after processing MNPs as antigenic molecules, become active APCs, which through the production of various secondary mediators are capable to orchestrate further cell recruitment for immune responses.

CONCLUSIONS

The conformationally rigid α-*O*-glycoside **1** at present the only example of α-Tn antigen mimetic, was functionalized with an ω-phosphonate linker to give the phosphonate derivative **2** and this latter was efficiently employed to decorate magnetite/maghemite MNPs. The obtained biocompatible **GMNPs** showed two main features: an high density of mimetic residues (0.84 saccharidic residues/nm^2) and the proper magnetic and hyperthermic properties for a possible

use as heat mediators in the hyperthermia treatment of tumors. In addition, the high cristallinity and the value of the magnetic moment of **GMNPs** suggest their possible use as contrast agent for MRI. The biocompatible **GMNPs** obtained showed two main features: a high density of mimetic residues (0.84 saccharidic residues/nm^2) and magnetic properties suitable for application as heat mediators in the hyperthermia treatment of tumors. A further increase of the heat release capability could be realized by slightly increasing the average diameter of the inorganic core. In addition, the high cristallinity and the value of the magnetic moment of **GMNPs** suggest their possible use as contrast agent for MRI.

As multivalent carriers of α-Tn mimetic residues, **GMNPs** were tested *in vitro* to evaluate their effects on macrophage activation. Macrophages treated with the monovalent α-Tn-like compound **2, CMNPs** and **PEMNPs** (as controls), and with **GMNPs,** clearly showed the ability to endocyte only the two nanosystems and not the non conjugated antigen **2**. Noteworthy, macrophages were able to endocyte both **CMNPs** and **GMNPs** independently of the glycosyl-coating, but only **GMNPs**, which are the MNPs displaying α-Tn-like epitopes, were able to activate macrophage effector functions, inducing gene expression and protein release of the TNF-α. The levels of TNF-α gene expression stimulated by **GMNPs** (30 μg/ml) are comparable to those obtained with the golden standard LPS (0.1 μg/ml) thus demonstrating that a multivalent presentation of α-Tn-like epitopes is necessary for macrophages activation.

Concluding, the glycosyl MNPs we propose herein are original immunoactive tools which could find a practical application for a better understanding of the biological properties and applicability of MNPs.

MATERIALS AND METHODS

NMR spectra were recorded on a Varian Gemini 200 MHz, on a Varian Gemini 300 MHz, on a Varian Inova 400 MHz and on a Varian Mercury 400 MHz spectrometers. The NMR spectra were referenced to solvent. Mass spectra were recorded on an LCQ-FLEET ion trap Thermo Fischer mass spectrometer. ESI-MS analysis was performed both in positive or negative ion mode. Optical rotation measurements were carried out on a Jasco DIP-370 polarimeter. Average diameter and size distribution of the MNPs were determined by transmission electron microscopy (TEM), using a CM12 PHILIPS transmission electron microscope operating at 100 kV. Samples were prepared by drop drying a dilute suspension of MNPs in heptane onto 200 mesh carbon-coated copper grids. The recorded micrographs were further analyzed with the Image Pro-Plus® software. The mean diameter and size distribution of each sample were obtained from a statistical analysis over ca. 600 MNPs. Powder X-ray diffraction (XRD) measurements were carried out using a Bruker D8 Advance diffractometer equipped with Cu Kα radiation and operating in θ−2θ Bragg−Brentano geometry at 40 kV and 40 mA. Lattice parameters were evaluated on averaging over (400), (511) and (440) peaks. The determination of the mean crystallite diameter, d, was performed on the (400) peak using the Scherrer equation,$d = (0.9\lambda)/(\beta \cos\theta)$, where λ is the wavelength of the incident X-ray (1.54178 Å), θ the diffraction angle, and β the full-width at half-maximum.

Magnetic measurements were performed using a Quantum Design MPMS SQUID magnetometer operating in the 1.8 – 400 K temperature range with a magnetic field up to ± 5 T. Measurements were performed on MNPs dispersed in heptane. All data were corrected for the diamagnetic contribution of the sample holder and of the solvent, which were separately measured. ZFC-FC curves were recorded in the 2.5 – 300 K temperature range using a 5 mT

probe field. AC susceptibility curves were recorded with a 24 A/m field amplitude between 2.5 and 300 K in the 1 – 1000 Hz frequency range.

Hyperthermic characterization was carried out on 0.33 g of a solution of **NP5** in hexane (1.9% w/w) using a 6 KW Five-Celes MP6-400 alternating magnetic field generator. The frequency and field amplitude values used in this work (183 kHz, 11.0 kA/m) were chosen in order to operate under the physiological limit, $H \cdot \nu < 5 \cdot 10^9$ $Am^{-1}s^{-1}$.[29] The temperature was recorded during 300 s of magnetic field application using an optical fibre thermometer with a GaAs crystal with a sensibility of 0.1 K connected to a digital temperature recorder (Fotemp®). The SAR value was calculated using the equation $SAR = \frac{\sum_i m_i c_{pi}}{m_{Me}} \Delta T / \Delta t$, where ΔT is the temperature increase in the interval of time Δt, m_{Me} is the total mass of metal, m_i is the mass in g of the i-species and C_{pi} their specific heat. The sum is extended to all the *i* species involved in the heat exchange. Since the measurements are carried in non adiabatic conditions, the ΔT / Δt values were extrapolated for t → 0 from temperature kinetic curve, by considering the initial slope.

FTIR spectra were collected on a Perkin Elmer Spectrum BX. The sample powders were ground with KBr and pressed into a pellet. The determination of Fe, S and P content was performed on a Optima 2000 Perkin Elmer Inductively Coupled Plasma (ICP) Optical Emission Spectrophotometry (OES) Dual Vision.

Materials and Synthesis. All solvents were of reagent grade quality and purchased commercially. All starting materials were purchased commercially and used without further

purification.

Synthesis of the linker monoaminohexaethyleneglycol, **6**. Monoazidehexaethyleneglycol used as starting material was prepared following a reported procedure.[21] Then, triphenylphosphine (480 mg, 1.83 mmol) was added to an ice-cooled solution of monoazidehexaethyleneglycol (0.271 g, 0.88 mmol) in dry THF (2.5 mL). The solution was warmed at 45°C for 2h then H_2O (130 μL) was added. The reaction mixture was stirred for 15 h at 35°C then diluted with H_2O (6 mL) and washed with toluene (2 x 4 mL). Evaporation of the aqueous layer under reduced pressure gave **6** (240 mg, 97%) as a pale yellow oil. The spectroscopic and analytical data were in agreement with those reported previously.[21]

Synthesis of the glycosyl derivative **7**. The glycosylsilylidene **3**[20] (0.753 g, 1.34 mmol) was dissolved into a freshly prepared solution of tributylamine hydrofluoride in THF (14.0 mL, 1M). The reaction mixture was stirred for 1 h at rt and then concentrated to dryness. The residue was dissolved in CH_2Cl_2 (8 mL) and then pyridine (3.3 mL, 40.2 mmol), acetic anhydride (1.27 mL, 13.4 mmol) and 4-dimethylaminopyridine (33 mg, 0.27 mmol) were added. The reaction mixture was stirred at rt for 10' and then diluted with CH_2Cl_2 (200 mL) and washed with water (2 x 20 mL), a 3% solution of HCl (2 x 20 mL) and a saturated solution of Na_2CO_3 (2 x 20 mL). The organic phase was dried over Na_2SO_4, filtered and concentrated to dryness. The crude was purified by flash column chromatography on silica gel (CH_2Cl_2/Acetone, 7/1) to give **4** (0.618 g, 85%) as a white solid. To a solution of **4** (0.201 g, 0.36 mmol) in THF (14 mL), H_2O (0.200 ml) and 10% Pd/C (140 mg, 0.04 mmol) were added. The mixture was stirred at rt under H_2 atmosphere for 2.5 h and then filtered through a pad of Celite®. Evaporation of the solvent under vacuum gave 185 mg of crude **5** which was used for the following reaction without any further purification. To a stirred solution of *O*-(benzotriazol-1-yl)-*N,N,N′,N′*-tetramethyluronium

tetrafluoroborate (234 mg, 0.73 mmol) in dry DMF (7 mL), 4-methylmorpholine (80 μL, 0.73 mmol) was added. The solution was stirred for 20 minutes at rt then a solution of **5** (185 mg) in dry DMF (3.6 mL) was added. The reaction mixture was stirred for 20' at rt then a solution of linker **6** (0.100 g, 0.360 mmol) in dry DMF (1.6 mL) was added. The reaction mixture was stirred for 1h at rt then concentrated to dryness. The crude was purified by flash chromatography on silica gel ($CHCl_3$/MeOH, 12/1 → 9/1) to give **7** (192 mg, 73%) as a pale yellow oil.

Synthesis of the compound **8**. To a stirred solution of **7** (0.049 g, 0.068 mmol) in dry CH_2Cl_2 (2 mL), triphenylphosphine (0.025 g, 0.095 mmol) and CBr_4 (0.027 g, 0.081 mmol) were added. The mixture was stirred at rt overnight then concentrated to dryness. The crude was purified by flash chromatography on silica gel ($CHCl_3$/MeOH, 30/1 → 9/1) to give **8** (47 mg, 88%).

Synthesis of compound **9**. Compound **8** (0.094 g, 0.12 mmol) was dissolved in tris-trimethysilylphosphite (1.0 mL, 2.99 mmol) under N_2 atmosphere. The reaction mixture was warmed at 110°C and stirred for 18h then concentrated to dryness to give **9** (95 mg, quantitative) as a glassy white solid.

Synthesis of phosphonate **2.** To a stirred solution of **9** (0.095 g, 0.120 mmol) in MeOH (10 mL), a 2.0 M solution (4 mL) of NH_3 in MeOH was added. The reaction mixture was stirred at rt overnight then concentrated to dryness to give **2** (79 mg) as a white hygroscopic solid. Phosphonate **2** was used for the following reaction without any further purification.

Synthesis of magnetite nanoparticles. Magnetite MNPs were synthesized using a seed-mediated growth process based on the Sun's method.[22] A solution of iron (III) acetylacetonate (0.96 g, 2.73 mmol), oleylamine (2.20 g, 8.21 mmol), oleic acid (2.33 g, 8.25 mmol), 1,2-

hexadecanediol (3.53 g, 13.65 mmol) in 1-octadecene (20 mL) was stirred at rt under a nitrogen flow for 1h, then heated to reflux (ca. 320°C) at a rate of 5°C/min and maintained at that temperature for 3h. The mixture was cooled to room temperature and diluted with a 1:1 toluene/heptane solution (10 mL). The mixture was treated with a 1:1 ethanol/isopropanol solution and the precipitated material was recovered using a permanent magnet. The obtained black powder was washed several times with ethanol and then re-dispersed in heptane. This solution was centrifuged at 2500 rpm for 15 min. Ethanol was added to the supernatant and 7 nm NPs were separated using a permanent magnet and then vacuum dried.

The obtained NPs were used as seeds to grow larger MNPs in a second thermal decomposition reaction: the MNPs (0.080 g) were mixed with iron (III) acetylacetonate (0.601 g, 1.68 mmol), oleylamine (1.92 g, 7.18 mmol), oleic acid (1.58 g, 5.59 mmol), 1,2-hexadecanediol (2.22 g, 8.60 mmol) in 1-octadecene (20 mL). Larger particles, **NP5**, were obtained following the same procedure described above. The obtained MNPs were dispersed in chloroform (16 mg/mL) for long term storage.

Synthesis of glycosyl magnetic nanoparticles, **GMNPs**. MNPs **NP5** (47.2 mg) were added to a solution of **2** (25 mg, 0.038 mmol) in 4.4 mL of 10:1 chloroform/methanol, and the mixture was mechanically stirred at 48°C for 48h. Methanol was then added to the mixture causing precipitation of MNPs. The product was washed with methanol and chloroform in order to remove unbound ligand and oleate-coated MNPs and then was vacuum dried. The product was dispersed in water by sonication. The solution was separated from the precipitate in order to collect only the water soluble MNPs. The recovered solution was then freeze-dried leading to a black-brown powder of glycosylated MNPs, **GMNPs**.

In order to improve the water solubility of the MNPs obtained, 1.5 mg of **GMNPs** were mixed with phosphonate **2** (1 mg, 0.0015 mmol) in mQ water (0.8 mL) and stirred at 45°C for 48h. MNPs were magnetically decanted and washed twice with water to remove the unbound ligand.

Synthesis of citrate-coated MNPs, **CMNPs.** In a round bottom flask a 1:1 solution of 1,2-dichlorobenzene/DMF (2.5 mL) was stirred under a nitrogen flow for 30', then **NP5** (19.3 mg) and monohydrated citric acid (20 mg, 0.05 mmol) were added. The reaction mixture was stirred under a blanket of nitrogen at 100°C, for 23h. After cooling at rt, ethyl ether was added and the dark-brown material was magnetically decanted. MNPs were washed three times with acetone and then vacuum dried.

Biological Tests. To measure the biological effects of MNPs, either functionalized or not functionalized with the α-Tn mimetic antigen, the concentration of each compound was expressed as μg/ml. To allow an easy comparison among compounds the correspondence between mass and mole concentrations was also calculated (see Table 1).

Table 1 Relationship between mass and mole concentrations of the tested compounds

	Compound (μg/ml)	**α-Tn-epitope mimetic (μM)**
2	1	1.5
CMNPs	1	—

GMNPs	1	0.2

Cell culture. The RAW 264.7 murine macrophage cell line (ATCC TIB-71; American Type Culture Collection, Manassas, VA, USA) was cultured in high glucose (4.5 g/l) Dulbecco's modified Eagle's medium (DMEM) supplemented with 10% heat-inactivated fetal bovine serum (FBS), 2mM L-glutamine, 100 IU/ml penicillin and 100 μg/ml streptomycin (Lonza, Milan, Italy) and kept in a 37 °C incubator with 5% CO_2. Cells were grown in 75-cm^2 flasks and sub-cultured by scraping when they reached 90% confluence with a 1:5 or 1:10 ratio in fresh medium. Before each experiment, viable cell count was assessed by trypan blue staining; thereafter cells were seeded and rendered quiescent by 18h serum deprivation.

Limulus amebocyte lysate (LAL) assay. LPS levels in each compound were measured in duplicate in serial 1:10 dilutions of each sample made with pyrogen-free water using a chromogenic LAL assay (Lonza, Basel, Switzerland), according to the manufacturer's protocol. The sensitivity of the LAL assay was 0.01 ng/ml.

MTT assay. Cell viability was measured by the 3-(4,5-dimethylthiazol-2-yl)-2,5-diphenyl-tetrazolium bromide (MTT) assay, as previously described (Lombardi et al., 2002). Briefly, RAW 264.7 cells were seeded in 24-well plates and treated with increasing concentrations (0.01-30 μg/ml) of **2**, **PEMNPs**, **CMNPs**, **GMNPs** or **GlcMNPs** for 24, 48 and 72 h at 37° C in a 5% CO_2 humidified incubator. The percentage of cell viability was calculated as (x × 100)/y, where x, and y were the absorbance read in compound-treated, and compound-untreated cells, respectively.

Calcein-AM assay. RAW 264.7 cells were labelled with 1 μM Calcein-AM (CAM) (Molecular Probes, Invitrogen) in serum-free PBS for 15 min at 37° C in the dark. After being washed, labelled cells were seeded in 24-well plates and allowed to adhere over-night at 37° C in a humidified incubator. The day after, RAW 264.7 cells were treated with increasing concentrations (0.01-30 μg/ml) of **2**, **PEMNPs**, **CMNPs**, **GMNPs** or **GlcMNPs** for 24, 48 and 72 h at 37° C in a 5% CO_2 humidified incubator. After incubation time the cells of each well were harvested, washed, labelled with propidium iodide (PI), and the viability was measured by flow cytometry. Lived cells were identified as CAM^{high}/PI^{-} population whereas dead cells were CAM^{low}/PI^{+}. Viability was calculated by FACSDiva software and expressed as the percentage of CAM^{high}/PI^{-} population relative to untreated cells.

Trypan blue-exclusion assay of cell viability. RAW 264.7 cells were seeded in 24-well plates and treated with increasing concentrations (0.01-30 μg/ml) of **2**, **PEMNPs**, **CMNPs**, **GMNPs** or **GlcMNPs**, for 24, 48 and 72 h at 37° C in a 5% CO_2 humidified incubator. After incubation time cells were harvested, stained with a trypan blue solution and counted under an inverted microscope. The percentage of cell viability was calculated as (x × 100)/y, where x, and y were the number of live and total cells in the same sample, respectively.

Qualitative study of MNPs uptake. RAW 264.7 cells (5 x 10^4 cells/well) were allowed to adhere overnight on sterile glass cover slips in 24-well culture plates and treated with **PEMNPs**, **CMNPs**, **GMNPs** or **GlcMNPs** (30 μg/ml) in complete medium for 24h at 37°C, 5% CO_2. The cover slips were washed twice with ice-cold PBS to remove unbound MNPs and cells were fixed with 4% paraformaldehyde for 15 min at 4° C. After two additional PBS washing, cells on the cover slips were stained with fresh prepared Prussian blue reagent (2% potassium

ferrocyanide [Sigma Aldrich]/12% HCl, 1:1, v/v) for 30 min. The cells were washed five times with PBS, and subsequently the cover slips were mounted on glass slides by SlowFade® reagent (Invitrogen, Milano, Italy). Cells were then observed by an inverted optical microscope (objective x 40) with an integrated camera (Motic AE2000 with integrated Moticam 3.0).

Quantitative study of MNPs uptake. RAW 264.7 cells were seeded (1 x 10^5 cells/well) in 12-well culture plates and treated with **2**, **PEMNPs**, **CMNPs**, **GMNPs** or **GlcMNPs** (30 μg/ml) for 24 h at 37° C in a 5% CO_2 humidified incubator. Following incubation, cells were washed twice with cold PBS to remove unbound MNPs, gently scraped from the culture plates on ice, and centrifuged (900 rpm, 5 min, 4°C). Cell pellets were resuspended in 200 μl PBS containing 2% FBS and analyzed by FACScalibur (FACS-Vantage, BD Bioscience, Milan). A total of 5000 viable cells were collected for each sample. For calculation cell debris and free particles were excluded by an electronical gate containing RAW 264.7 cells of all size and granularities in a FSC-SSC-histogram. Univariant histograms of SSC determined the mean of cell granularity used as measure of uptake by RAW 264.7 cells. Data were analyzed by using FACSDiva software (BD Bioscience, Milan).

For uptake time-course determination, RAW 264.7 cells were seeded (1 x 10^5 cells/well) in 12-well culture plates and incubated with **2**, **PEMNPs**, **CMNPs**, **GMNPs** or **GlcMNPs** (30 μg/ml) for up to 72 h at 37° C in a 5% CO_2 humidified incubator. At different incubation times (1, 3, 6, 18, 24, 48 and 72h) cell samples were harvested, prepared and analyzed by FACS, as described above.

To explore the relationship between cellular uptake and compound concentration RAW 264.7 cells were seeded in 12-well culture plates and incubated with increasing concentrations (0.1-30

μg/ml) of **2**, **PEMNPs**, **CMNPs**, **GMNPs** or **GlcMNPs** for 24, 48, and 72 h at 37° C in a 5% CO_2 humidified incubator. Following incubation cell samples were harvested, prepared and analyzed by FACS, as described above.

RT-PCR. RAW 264.7 cells were seeded (1 x 10^6 cells/well) in 6-well culture plates and treated with increasing concentrations (1-30 μg/ml) of **2**, **PEMNPs**, **CMNPs**, **GMNPs** or **GlcMNPs** for 24 h at 37° C in a 5% CO_2 humidified incubator. Bacterial LPS (0.1 μg/ml)-treated and -untreated cells were used as positive and standard controls, respectively, for RT-PCR analysis. Total RNA was isolated using the GenElute™ mammalian total RNA kit (Sigma Aldrich, Milan) and reverse-transcribed to cDNA using ThermoScript RT-PCR™ kit (Invitrogen, Milan, Italy), according to the manufacturer's instructions. For amplification, 3 μl of cDNA were added to GoTaq FlexiDNA Polymerase (Promega, Milan, Italy) in 25 μl reaction buffer, containing 0.5 μM of forward and reverse primers (Table 1S, Supplementary Information). Amplification products were resolved in 1% agarose gel by electrophoresis and visualized with ethidium bromide. Signals were quantified with densitometric analysis software (NIH Image 1.32; Bethesda, MD, USA). Data were expressed as the ratio of the signals obtained for each gene in one sample divided by that obtained for the reference gene (mouse β-actin) in the same sample.

TNF-α release. RAW 264.7 cells were seeded in 24-well culture plates and treated with increasing concentrations (0.1-30 μg/ml) of **2**, **PEMNPs**, **CMNPs**, **GMNPs** or **GlcMNPs** for 24, 48 and 72 h at 37° C in a 5% CO_2 humidified incubator. Bacterial LPS (0.1 μg/ml)-treated cells, and -untreated cells were used as positive and standard controls, respectively, of TNF-α release. At the end of each experiment, supernatants were collected and stored at −20 °C until

assays. The amounts of TNF-α in cell culture media were assayed using enzyme-linked immunosorbent assay (ELISA) kits (Biolegend, San Diego, USA), according to the manufacturer's instructions. The concentrations of TNF-α in the samples were determined by extrapolation from specific reference standard curves.

Statistical analysis. Results were expressed as means ± SEM of at least three independent experiments run in triplicate. Statistical significance was evaluated by the one-way ANOVA followed by Student's t-test for unpaired populations (Graph Pad Software, Inc., San Diego, USA). Differences were considered statistically significant when $p \leq 0.05$.

Acknowledgment. The authors gratefully acknowledge Maria Francesca Casula for DLS and Z-potential measurements. The MIUR through FIRB project RBAP114AMK and PRIN project 2010 JMAZML_009- RI.NA.ME. "Rete Integrata per la Nanomedicina", AIRC (grant 2012), Ente Cassa di Risparmio di Firenze and COST Action CM1102 "MultiGlycoNano" are acknowledged for financial support.

Supporting Information Available: Optical rotation and spectroscopic data for all compounds; Selected TEM images of **MNP**s, **CMNP**s and **GMNP**s; XRD patterns and FTIR spectra of MNPs coated with surfactant and with the α-Tn mimetic; MNP magnetic properties; This material is available free of charge via the Internet at http://pubs.acs.org.

REFERENCES AND NOTES

1. Guo, Z.; Wang, Q. Recent development in carbohydrate-based cancer vaccines. *Curr. Opin. Chem.*

Biol. **2009**, *13*, 608-17.

2. Liu, C.C.; Ye, X.S.; Carbohydrate-based cancer vaccines: target cancer with sugar bullets. *Glycoconj J.* **2012**, *29*, 259-71.

3. Parry, A.L.; Clemson, N.A.; Ellis, J.; Bernhard, S.S.; Davis, B.G.; Cameron, N.R. 'Multicopy multivalent' glycopolymer-stabilized gold nanoparticles as potential synthetic cancer vaccines. *J Am Chem Soc.* **2013**, *135*, 9362-5.

4. Reddy, S.T.; Swartz, M.A.; Hubbell, J.A. Targeting dendritic cells with biomaterials: developing the next generation of vaccines. *Trends Immunol.* **2006**, *27*, 573-9.

5. Hirosue, S.; Kourtis, I.C.; van der Vlies, A.J.; Hubbell, J.A.; Swartz, M.A. Antigen delivery to dendritic cells by poly(propylene sulfide) nanoparticles with disulfide conjugated peptides: Cross-presentation and T cell activation. *Vaccine* **2010**, *28*, 7897-906.

6. Molino, N.M.; Anderson, A.K.; Nelson, E.L.; Wang, S.W. Biomimetic Protein Nanoparticles facilitate Enhanced Dendritic Cell Activation and Cross-Presentation *ACSNano* **2013**, DOI: 10.1021/nn403085w.

7. Brokx, R.D.; Bisland, S.K.; Gariépy, J. Designing peptide-based scaffolds as drug delivery vehicles. *J. Control Release* **2002**, *78*, 115-23.

8. Darbre, T.; Reymond, J.L. Glycopeptides for Biomedical applications. *Curr. Top. Med. Chem.* **2008**, *8*, 1286-93.

9. Marradi, M.; Chiodo, F.; Garcia, I.; Penadés, S. Glyconanoparticles as multifunctional and multimodal carbohydrate systems. *Chem Soc. Rev.* **2013**, *42*, 4728-45.

10. Pankhurst, Q. A.; Connolly, J.; Jones, S. K.; Dobson, J. Applications of magnetic nanoparticles in

biomedicine *J. Phys. D: Appl. Phys.* **2003**, *36* R167-81.

11. Johannsen, M.; Gneveckow, U.; Taymoorian, K.; Thiesen, B.; Waldöfner, N.; Scholz, R.; Jung, K.; Jordan, A.; Wust, P.; Loening, S. A. Morbidity and Quality of Life During Thermotherapy Using Magnetic Nanoparticles in Locally Recurrent Prostate Cancer: Results of a Prospective Phase I Trial. *Int. J. Hyperthermia* **2007**, *23*, 315-23.

12. Maier-Hauff, K; Ulrich, F.; Nestler, D.; Niehoff, H.; Wust, P.; Thiesen, B.; Orawa, H.; Budach, V ; Jordan, A. Efficacy and safety of intratumoral thermotherapy using magnetic iron-oxide nanoparticles combined with external beam radiotherapy on patients with recurrent glioblastoma multiforme *J. Neurooncol*. **2011**, *103*, 317–24.

13. Frey, B.; Weiss, E.-M.; Rubner, Y.; Wunderlich, R.; Ott, O. J.; Sauer R.; Fietkau, R.; Gaipl, U. S. Old and new facts about hyperthermia-induced modulations of the immune system. *Int. J. Hyperthermia* **2012**, *28*, 528–42.

14. Hollingsworth, M. A.; Swanson, B. J. Mucins in cancer: protection and control of the cell surface. *Nature Reviews Cancer* **2004**, *4*, 45.

15. Tatsushi, T.; Singhal, A.K. Synthetic Carbohydrates vaccines based on tumor-associated antigens. *Chem. Soc. Rev.* **1995**, 24, 231-42

16. Ingale, S.; Wolfert, M.A.; Gaekwad, J.; Buskas, T.; Boons, G.J. Robust immune response elicited by a fully synthetic three-component vaccine. *Nat. Chem. Biol.* **2007**, *10*, 663-7.

17. Corzana, F.; Busto, J.H.; Jimenéz-Osés, G.; Asensio, J.L.; Jimenéz-Barbero, J.; Peregrìna, J.M.; Avenoza, A. New insights into alpha-GalNAc-Ser motif: Influence of hydrogen bonding versus solvent interactions on the preferred conformation *J. Am. Chem. Soc.* **2006**, *128,* 14640-8

18. Coltart, D.M.; Royyuru, A.K.; Williams, L.J.; Glunz, P.W.; Sames,D.; Kuduk, S.D.; Schwarz, J.B;

Chen, X.-T.; Danishefsky, S.J.; Live, D.H. Principles of mucin architecture: structural studies on synthetic glicopeptides bearing clustered mono-, di-, tri- and hexasaccharide glycodomains. *J. Am. Chem. Soc.* **2002**, *124*, 9833-44.

19. Capozzi, G.; Franck, R.W.; Mattioli, M.; Menichetti, S.; Nativi, C.; Valle, G. Phthalimidesulphenyl chloride part 9. A simple access to α,α'-dioxothiones, a new class of bis-heterodienes. Synthesis of 1,4-oxathiin systems. *J. Org. Chem.* **1995**, *60*, 6416-26.

20. Jimenéz-Barbero, J.; Dragoni, E.; Venturi, C.; Nannucci, F.; Ardà, A.; Fontanella, M.; André, S.; Cañada, F.J.; Gabius, H.-J.; Nativi, C. Alpha-O-linked glycopeptide mimetics: synthesis, conformation, analysis and interactions with Viscumin, a galactoside-binding model lectin. *Chemistry Eur. J.* **2009**, *15*, 10423-31.

21. Menger, F.; Hailing Zhang, M. Self-Adhesion among Phospholipid Vesicles. *J. Am. Chem. Soc.* **2006**, *128*, 1414-15.

22. Sun, S.; Zeng, H. Size-Controlled Synthesis of Magnetite Nanoparticles *J. Am. Chem. Soc.* **2002**, *124*, 8204-5.

23. Kwon, S.G.; Piao, Y.; Park, J.; Angappane, S.; Jo, Y.; Hwang, N.-M.; Park, J.-G.; Hyeon T.; Kinetics of Monodisperse Iron Oxide Nanocrystal Formation by "Heating-Up" Process *J. Am. Chem. Soc.* **2007**, *129*, 12571-84.

24. Kwon, S. G.; Hyeon, T. Kinetics of Monodisperse Iron Oxide Nanocrystal Formation by "Heating-up" Process. *Acc. Chem. Res.* **2008**, *41*, 1696–1709.

25. Chen, C.-J.; Chiang, R.-K.; Lai, H.-Y.; Lin, C.-R. Characterization of Monodisperse Wüstite Nanoparticles Following Partial Oxidation. *J. Phys. Chem. C* **2010**, *114*, 4258–63.

26. Néel, L."Théorie du traînage magnétique des ferromagnétiques en grains fins avec applications aux

terres cuites" *Ann. Geophys.* **1949**, *5*, 99-136.

27. Casula,M. F.; Floris, P.; Innocenti, C.; Lascialfari, A.; Marinone, M.; Corti, M.; Sperling, R. A.; Parak, W. J.; Sangregorio, C. Magnetic Resonance Imaging Contrast Agents Based on Iron Oxide Superparamagnetic Ferrofluids. *Chem. Mater.* **2010**, *22*, 1739-48.

28. Cornell, R. M.; Schwertmann, U. The Iron Oxides; VCH: Weinheim, Germany, 1996.

29. Hergt, R.; Dutz, S. Magnetic Particle Hyperthermia—Biophysical Limitations of a Visionary Tumor Therapy. *J. Magn. Magn. Mater.* **2007**, *311*, 187-92.

30. Lartigue, L.; Innocenti, C.; Kalaivani, T.; Awwad, A.; del Mar Sanchez, M.; Guari, Y.; Larinova, J.; Guérin, C.; G. Montero, J. L.; Barragan-Montero, V.; Arosio, P.; Lascialfari, A.; Gatteschi, D.; Sangregorio, C.; Water-Dispersible Sugar-Coated Iron Oxide Nanoparticles. An Evaluation of their Relaxometric and Magnetic Hyperthermia Properties." *J. Am. Chem. Soc.* **2011,** 133, 10459-72.

31. Shafi, K.V.P.M.; Ulman, A.; Yan, X.; Yang, N.L.; Estournes, C.; White, H. Rafailovich, M. Sonochemical Synthesis of Functionalized Amorphous Iron Oxide Nanoparticles *Langmuir* **2001**, *17*, 5093–7.

32. Lartigue, L.; Oumzil, K.; Guari, Y.; Larionova, J.; Guérin, C.; Montero, J.-L.; Barragan-Montero, V.; Sangregorio, C.; Caneschi, A.; Innocenti, C.; Kalaivani, T.; Arosio, P.; Lascialfari, A. Water-Soluble Rhamnose-Coated Fe_3O_4 Nanoparticles *Org. Lett.* **2009**, *11*, 2992-5.

33. Barja, B.C.; Tejedor-Tejedor, M. I.; Anderson, M. A. Complexation of Methylphosphonic Acid with the Surface of Goethite Particles in Aqueous Solution. *Langmuir* **1999**, *15*, 2316-21.

34. Fallarini, S.; Paoletti, T.; Battaglini, C.O.; Ronchi, P.; Lay, L.; Bonomi, R.; Jha, S.; Mancin, F.; Scrimin, P.; Lombardi, G. Factors affecting T cell responses induced by fully synthetic glyco-gold-nanoparticles. *Nanoscale* **2013**, *5*, 390-400.

35. Adams, D.O.; Hamilton, T.A. The cell biology of macrophage activation. *Ann. Rev. Immunol.* **1984**, *2*, 283-318.

36. Paoletti, T.; Fallarini, S.; Gugliesi, F.; Minassi, A.; Appendino, G.; Lombardi, G. Anti-inflammatory and vascularprotective properties of 8-prenylapigenin. *Eur. J. Pharmacol.* **2009** *620*, 120-30.

37. Kunzmann, A.; Andersson, B.; Thurnherr, T.; Krug, H.; Scheynius, A.; Fadeel, B. Toxicology of engineered nanomaterials: focus on biocompatibility, biodistribution and biodegradation. *Biochim Biophys Acta* **2011**, *1810*, 361-73.

38. Metz, S.; Bonaterra, G,; Rudelius, M.; Settles, M.; Rummeny, E.J.; Daldrup-Link, H.E. Capacity of human monocytes to phagocytose approved iron oxide MR contrast agents in vitro *Eur. Radiol.* **2004**, *14*, 1851-8.

39. Allard-Vannier, E.; Cohen-Jonathan, S.; Gautier, J.; Hervé-Aubert, K.; Munnier, E.; Soucé, M.; Legras, P.; Passirani, C.; Chourpa, I. Pegylated magnetic nanocarriers for doxorubicin delivery: a quantitative determination of stealthiness in vitro and in vivo *Eur. J. Pharm. Biopharm.* **2012**, *81*, 498-505.

40. Moros, M.; Hernáez, B.; Garet, E.; Dias, JT.; Sáez, B.; Grazú, V.; González-Fernández, A.; Alonso, C.; de la Fuente, J.M. Monosaccharides versus PEG-functionalized NPs: influence in the cellular uptake. *ACS Nano.* **2012,** 6, 1565-77.